2012

Novel SrTi1-xFexO3 nanocubes synthesized by microwave-assisted hydrothermal method

CRYSTENGCOMM, CAMBRIDGE, v. 14, n. 11, supl. 1, Part 3, pp. 4068-4073, JUL, 2012
http://www.producao.usp.br/handle/BDPI/34346

CrystEngComm

Cite this: *CrystEngComm*, 2012, **14**, 4068–4073

www.rsc.org/crystengcomm

PAPER

Novel $SrTi_{1-x}Fe_xO_3$ nanocubes synthesized by microwave-assisted hydrothermal method†

Luís F. da Silva,*[a] Waldir Avansi Jr.,[b] Mário L. Moreira,[b] Juan Andrés,[c] Elson Longo[b] and Valmor R. Mastelaro[a]

Received 16th February 2012, Accepted 27th March 2012
DOI: 10.1039/c2ce25229e

We report herein for the first time a facile synthesis method to obtain $SrTi_{1-x}Fe_xO_3$ nanocubes by means by a microwave-assisted hydrothermal (MAH) method at 140 °C. The effect of iron addition on the structural and morphological properties of $SrTiO_3$ was investigated. X-ray diffraction measurements show that all STFO samples present a cubic perovskite structure. X-ray absorption spectroscopy at Fe absorption K-edge measurements revealed that iron ions are in a mixed Fe^{2+}/Fe^{3+} oxidation state and preferentially occupy the Ti^{4+}-site. UV-visible spectra reveal a reduction in the optical gap (E_{gap}) of STFO samples as the amount of iron is increased. An analysis of the data obtained by field emission scanning electron microscopy points out that the nanoparticles present a cubic morphology independently of iron content. According to high-resolution transmission electron microscopy results, these nanocubes are formed by a self-assembly process of small primary nanocrystals.

1. Introduction

In recent years, strontium titanate ferrite $SrTi_{1-x}Fe_xO_3$ (STFO) solid solution has attracted the attention of the scientific community because STFO samples exhibit a p-type conducting behavior at high temperatures and may thus be applied in resistive gas sensor devices for oxygen and hydrocarbons.[1–4] Very recently, it was demonstrated that STFO samples also exhibit photocatalytic activity under visible radiation.[5] Brixner and co-workers[6] were the first to report the synthesis of STFO using a solid-state reaction (SSR) procedure which requires temperatures around 1100 °C and sintering times between 10 and 14 h.[6] This methodology has been commonly employed to prepare STFO powders used to prepare thick and/or thin films to be applied in gas sensors.[2,3,7,8]

An alternative way to decrease the grain size consists of submitting samples prepared by the SSR procedure to a ball milling. Hu and co-workers[9] reported results obtained for undoped $SrTiO_3$ samples submitted to ball milling processing. These authors obtained smaller nanoparticles of *ca.* 27 nm, though the samples require a long period of milling of 120 h.

The ability to design and control crystallinity, structure and morphology at the nanometer and micrometer scale is one of the most fundamental challenges in condensed matter science,[10–14] mainly due to the strong correlation between these factors, their properties and widespread technological applications.[15–22]

Recently, we demonstrated that the photoluminescent property of undoped $SrTiO_3$ powders was significantly enhanced by a reduction in particle size.[23] Usually, the synthesis of oxide compounds is conducted by a polymeric precursor method,[24] sol–gel[25] or conventional hydrothermal process.[26] High temperatures and/or long treatment times are required when using these methods. Currently, modification of energy and time-consuming processes are valuable for research in materials science, especially for the synthesis of inorganic compounds,[27] for which microwave heating has been used in recent years to lower the time and temperature of synthesis. The MAH method is considered as fast, clean, simple and often energetically more efficient when compared to the other above methods.[27] In 1992, Komarneni's group reported the use of the MAH method to synthesize binary oxide ceramic powders, such as $KNbO_3$ and $BaTiO_3$.[28] Following their research, the use of microwave radiation for the hydrothermal synthesis of oxide compounds increased rapidly over the past several years.[27,29–33] It has been also observed that microwave radiation is a powerful tool to accelerate the formation of metal oxide nanoparticles.[34] For example, Godinho and co-workers reported that the use of microwave irradiation during hydrothermal synthesis significantly decreases the treatment time required to obtain CeO_2:Gd nanorods.[30]

The MAH method combines effects of solvents, temperature and pressure on ionic reaction equilibrium and provides a

[a]*Instituto de Física de São Carlos, Universidade de São Paulo, Avenida Trabalhador São-carlense, 400, 13566-590, São Carlos, SP, Brazil. E-mail: lfsilva@ursa.ifsc.usp.br; Fax: +55 16 3373 9824; Tel: +55 16 3373 9828*
[b]*LIEC, Instituto de Química, Universidade Estadual Paulista, P.O. Box 355, 14800-900, Araraquara, SP, Brazil. Tel: +55 16 3301 6643*
[c]*Departamento de Química-Física y Analítica, Universitat Jaume I, Campus de Riu Sec, Castelló E-12080, Spain*
† Electronic supplementary information (ESI) available. See DOI: 10.1039/c2ce25229e

low-heating method to prepare different nano- or micro-sized oxide ceramic samples with controllable particle size and aggregation process.[27,29–32,35–37] Moreover, MAH-mediated synthesis also involves an acceleration of the kinetic process leading to the formation of particles with uniform dimensions.[34,37,38] Due to these factors the MAH method has been used in the synthesis of STFO solid solutions.

On the other hand, Alfredsson and co-workers conducted a theoretical and experimental study based on the $CaTiO_3$ perovskite and showed that the crystal morphology can also be varied by a suitable choice of dopant ions and their concentration.[39] They showed that dopant introduction is a alternative way to modify the relative energy of the different crystal faces, and consequently, to control the crystal morphology.[39]

Herein, we describe the synthesis of STFO solid solution using the MAH method, while studying the effect of iron content on the structural and morphological properties of $SrTiO_3$. X-ray diffraction (XRD), X-ray absorption spectroscopy (XANES and EXAFS regions), UV-visible absorption, field emission scanning electron microscopy (FE-SEM), and high resolution transmission electron microscopy (HRTEM) techniques were employed.

2. Experimental

2.1. Materials synthesis

STFO (x = 0, 5, 10, 25 and 40% mol) solid solutions were prepared according to the following methodology: first, $TiOSO_4 \cdot yH_2SO_4 \cdot yH_2O$ (99.9%) reagent was added into 50 mL of deionized water at 60 °C under stirring and purged with N_2 gas (12 cm^3 min^{-1}). $FeCl_3$ and $SrCl_2 \cdot 2H_2O$ (both 99.9%) were dissolved in solution to obtain a 0.01 M solutions of each. Appropriate amounts of these solutions were then mixed to obtain a final solution with a molar ratio of Sr : (Ti + Fe) equal to 1 : 1. Finally, 50 mL of 6 M KOH (85%) was added to the solution under constant stirring and nitrogen flux. The KOH acts as a mineralizer, favoring the co-precipitation of Sr, Ti and Fe hydroxides which will form the precursor solution. All reagents were obtained from Aldrich Company.

The final solution was then placed in a 110 mL Teflon autoclave which was closed and inserted in the MAH system operated at a frequency of 2.45 GHz with a maximum power of 800 W. The final solution was heated at 140 °C for 10 min at a heating rate of 140 °C min^{-1} without stirring and under a constant pressure of 3 bar. After the synthesis, the autoclave was cooled naturally to room temperature. The precipitated powders were removed and washed with deionized water and isopropyl alcohol several times until a neutral pH was attained. The powder sample was then dried at 80 °C for 12 h.

2.2. Material characterization

XRD patterns were collected in a Rigaku diffractometer (Rotaflex, RU200B), operating in Bragg configuration using Cu-Kα radiation from 20 to 100° with a 0.02° step width and a scanning rate of 5 s per point. The lattice parameter, a, was calculated from the (110) peak using Bragg's law.[40]

To evaluate the iron oxidation state and its site occupation in the $SrTiO_3$ lattice, X-ray absorption spectroscopy (XAS) measurements were performed at the D04B-XAS1 beamline on the Brazilian Synchrotron Light Laboratory (LNLS). The experiments were carried out at the Fe K-edge (7112 eV) in a transmission mode at room temperature using a Si(111) channel cut monochromator. X-ray absorption near-edge structure (XANES) spectra were collected for each sample between 7090 and 7190 eV using energy steps of 0.5 eV. For comparison purposes, all spectra were background removed and normalized using as unity the first EXAFS (extended X-ray absorption fine structure) oscillation. To determine the Fe oxidation state from Fe K-edge XANES spectra, the integration method proposed by Olimov and co-workers was used.[41]

Fe K-edge EXAFS spectra were recorded between 7100 and 7900 eV with energy steps of 2 eV. EXAFS spectra were processed using the Multiplatform Applications for XAFS code (MAX).[42] The theoretical EXAFS spectra of STFO (x = 0.25) sample was calculated with the *ab initio* FEFF8.3 code[43] with the structural parameters determined by XRD.

UV-visible spectra of STFO samples were recorded using a Cary 5G spectrometer in the total reflection mode by the integration sphere, and the optical gap (E_{gap}) was estimated using the Wood and Tauc method.[44]

Morphological properties of the STFO samples were characterized using FE-SEM (Zeiss Supra35) operating at 5 kV in different magnification. The microanalysis by energy-dispersive X-ray (EDX) spectroscopy was performed in a spectrometer EDAX-AMETEC (model APPOLLO X). TEM and HRTEM images were obtained on a JEOL (JEM, 2100 HT) microscope operating at 200 kV.

3. Results and discussion

All diffraction patterns of STFO samples shown in Fig. 1a were indexed to a cubic perovskite structure of $SrTiO_3$ with $Pm3m$ space group (Joint Committee on Powder Diffraction Standards (JCPDS) file No. 35-0734), except for the x = 0.4 sample which also shows diffraction peaks corresponding to the $SrCO_3$ phase (JCPDS file No. 05-0418). No diffraction peak related to iron oxide phases were observed which indicates that iron ions were homogeneously incorporated into the $SrTiO_3$ lattice. Cu-Kα_2 radiation diffraction was also observed in pure $SrTiO_3$ owing to the large crystallite size.

Fig. 1b shows that an increase in the iron content displaced the diffraction peaks to lower 2θ angles which indicates an increase in the lattice parameter, a, as can be observed from the analysis of the values reported in Table 1. This increase on the unit cell parameter is expected due to the partial substitution of Ti^{4+} by Fe^{2+} and/or Fe^{3+} ions (see below) which, according to Shannon and co-workers,[45] have ionic radii of = 0.605 Å (Ti^{4+}), 0.78 Å (Fe^{2+}) and 0.645 Å (Fe^{3+}), respectively. Some authors have reported contrary behavior of lattice parameter as a function of iron content.[3,6,46,47] This effect can be explained by the hydrothermal environment present an atmosphere with low amount of oxygen, which favors formation of reduced STFO samples.

The oxidation state of iron atoms was determined from the XANES spectra analysis measured at the Fe K-edge. Fig. 2a and b show the XANES spectra of iron-based reference compounds and XANES spectra of STFO samples, respectively. The pre-edge features presented on the XANES spectra of STFO samples

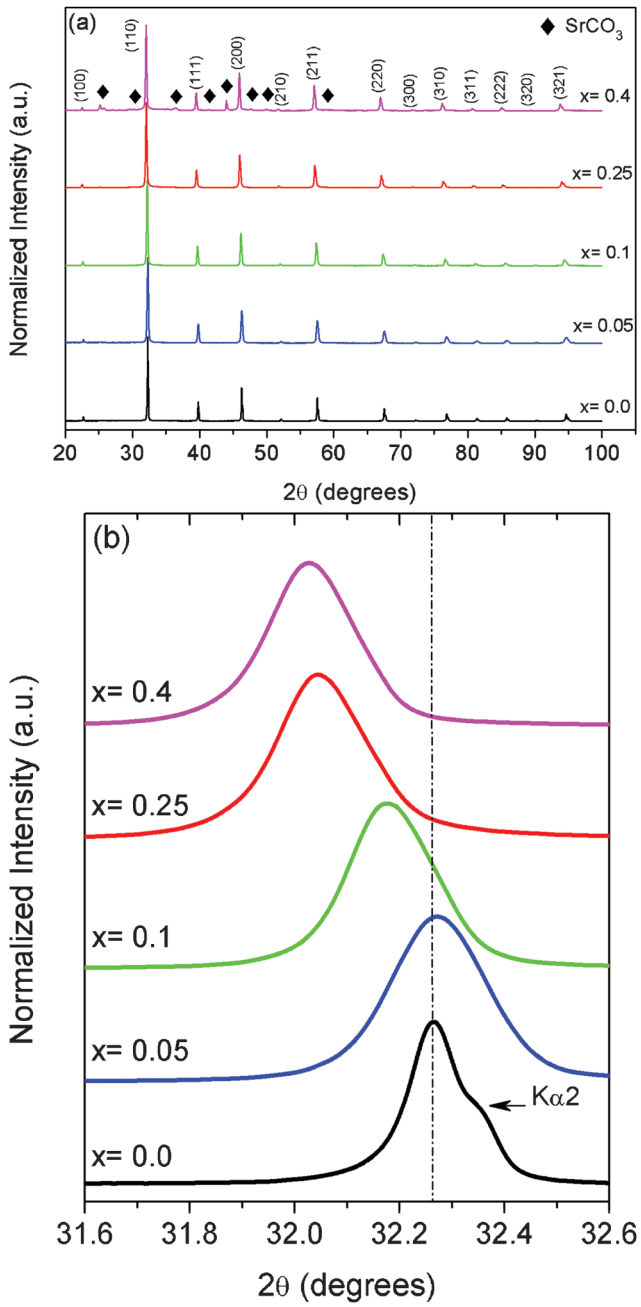

Fig. 1 (a) XRD patterns of $SrTi_{1-x}Fe_xO_3$ powder samples. (b) (110) diffraction peak shift as a function of iron content.

Table 1 Lattice parameter (±0.002 Å), oxidation state of iron (±0.3), and optical gap, determined for $SrTi_{1-x}Fe_xO_3$ samples synthesized by the MAH method

Fe content, x	Lattice parameter, a/Å	Fe oxidation state	Optical gap, E_{gap}/eV
0.0	3.920	—	3.25
0.05	3.919	2.30	3.04
0.1	3.931	2.31	3.05
0.25	3.946	2.29	2.92
0.4	3.948	2.30	2.87

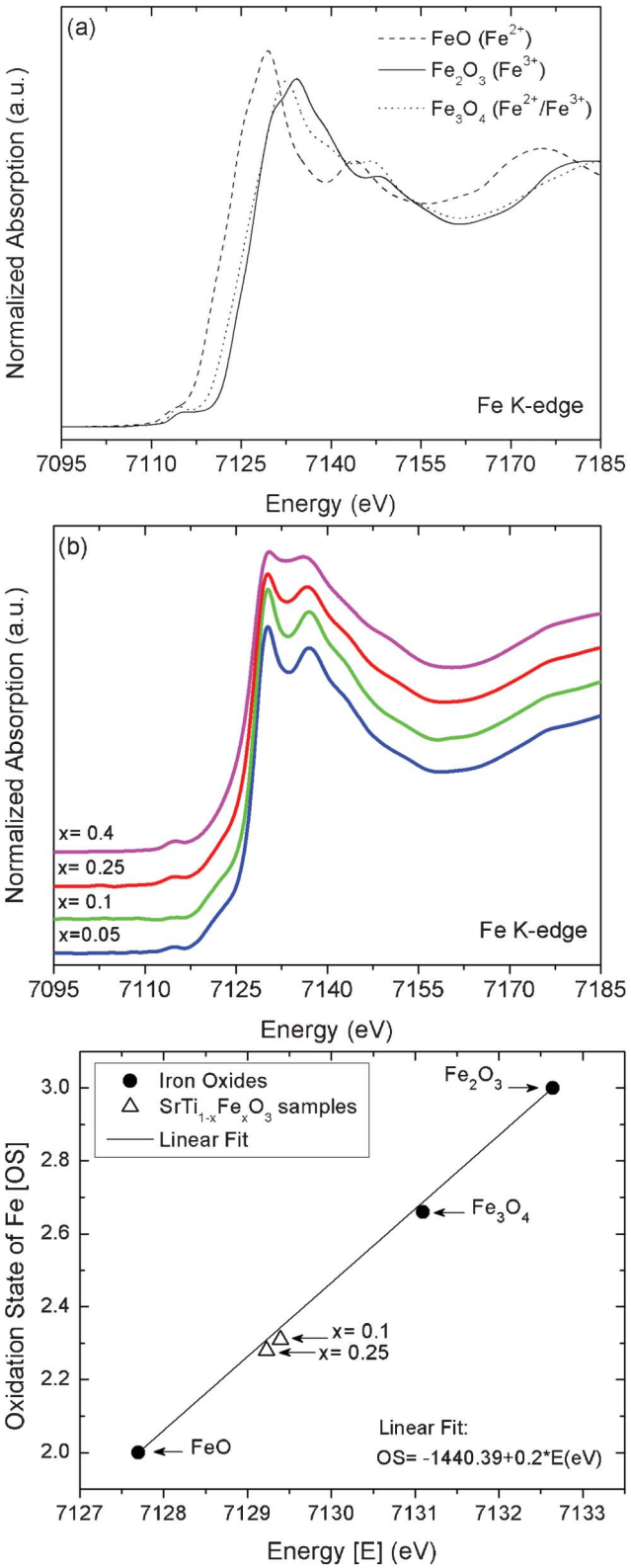

Fig. 2 XANES spectra at the Fe-K edge: (a) iron oxide standards (FeO, Fe_2O_3 and Fe_3O_4) used in the calibration procedure, (b) $SrTi_{1-x}Fe_xO_3$ samples and (c) Fe oxidation state in $SrTi_{1-x}Fe_xO_3$ samples determined using the integration method.[41]

are characteristic of six-coordinate iron compounds.[48] Furthermore, from these XANES spectra, the iron oxidation state was determined using the integration method.[41] Fig. 2c gives a mean value of 2.3 for the oxidation state of iron ions corresponding to a mixed valence of iron, *i.e.* Fe^{2+} and Fe^{3+} ions with a predominance of Fe^{2+} ions in all STFO samples.

To verify if Fe atoms are located at Ti sites, the EXAFS spectrum of the $x = 0.25$ sample was measured and compared to calculated EXAFS spectra. EXAFS spectra were calculated by supposing the substitution of either Sr or Ti by Fe atoms. Fig. 3a shows the comparison of calculated and experimental EXAFS spectra while the corresponding Fourier transform (FT) magnitudes are shown in Fig. 3b. The first FT peak corresponds to the first Fe–O coordination shell while the other peaks are related to further Fe-coordination shells.

As observed in Fig. 3a, the calculated EXAFS spectrum on the case of Fe ions located at Ti-sites is quite similar to the experimental EXAFS spectrum, whereas the EXAFS spectrum of Fe ions at Sr-sites is very different. An analysis and a comparison of FT curves also confirms that Fe ions are preferentially located at Ti sites (Fig. 3b).

As the Ti^{4+} ions are partly substituted by Fe^{2+} and Fe^{3+} ions, different types of defects are created,[49] mainly oxygen vacancies (Vö), due to charge compensation.[8] The unbalanced charges in FeO_6 octahedra may produce local polarization between two adjacent octahedra in different charge configurations.

Optical absorbance measurements of STFO ($x = 0.0$, 0.1 and 0.4) samples are shown in Fig. 4 as a function of iron content (the optical absorbance spectra of all STFO samples are illustrated in Fig. 1S, ESI†). An increase in the iron content causes an absorbance shift to lower energy which suggests the presence of a localized state inside the band gap.[50] The reduction on the optical gap (E_{gap}) with increasing x shown in Table 1 can be attributed to lattice defects and oxygen vacancies formed due to the substitution of Ti^{4+} by Fe^{2+} and Fe^{3+} ions.

Fig. 5 shows FE-SEM images of STFO samples and EDX spectrum of the $x = 0.25$ sample. An analysis of the images depicted in Fig. 5 clearly shows that the morphology of the samples is based on a cube shape. For the undoped sample ($x = 0.0$), FE-SEM images display poorly formed microcubes as a result of initial state of nanocube self-assembly. Moreover, an analysis of the results presented in Fig. 5b–e show that with an increase in the iron content, the formation of well defined cube nanoparticles occurs, with a reduction in particles size from *ca.* 1.5 μm ($x = 0.0$) to 90 nm ($x = 0.4$). The EDX spectrum depicted in Fig. 5f confirms Sr, Ti, Fe and O elements in the $x = 0.25$ sample. Similar results were observed for the other samples.

Fig. 6 shows TEM and HRTEM images of the $x = 0.4$ sample. The TEM image of Fig. 6a reveals that the nanocubes are formed by the aggregation of small nanocrystals of *ca.* 5 nm of diameter. An analysis of HRTEM images of region A shown in Fig. 6a indicates that the nanocrystal interplanar distance is *ca.* 0.28 nm which corresponds to the (110) crystallographic plane (Fig. 6c).[23]

Fig. 6b shows a TEM image of two nanocubes in the initial formation step while the HRTEM image (Fig. 6d) of region B in Fig. 6b shows a parallelism of the lattice fringes which also shows an interplanar distance related to the (110) crystallographic planes of a $SrTiO_3$ perovskite cubic structure.[23] The alignment along the same crystallographic direction indicates that the nanocubes have a mesocrystalline nature.[51–54] The lower

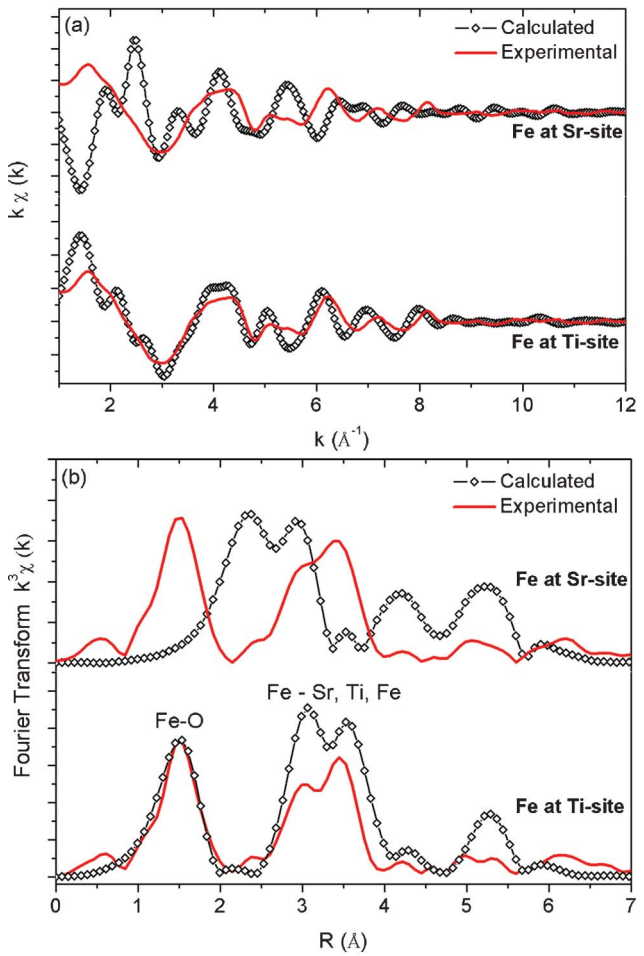

Fig. 3 Experimental and calculated EXAFS (a) and Fourier transform magnitude of the k^3-weighted EXAFS spectra (b) of $Sr_{0.75}Fe_{0.25}TiO_3$ and $SrTi_{0.75}Fe_{0.25}O_3$.

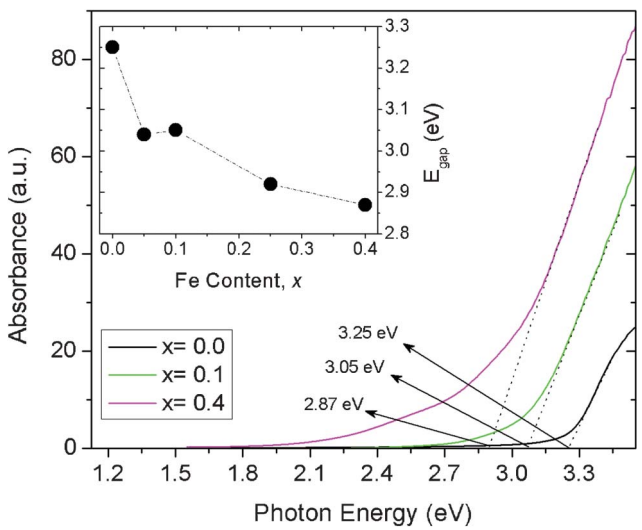

Fig. 4 Absorbance spectra of $SrTi_{1-x}Fe_xO_3$ ($x = 0.0$, 0.1 and 0.4) samples. The inset shows the optical gap (E_{gap}) as a function of iron content.

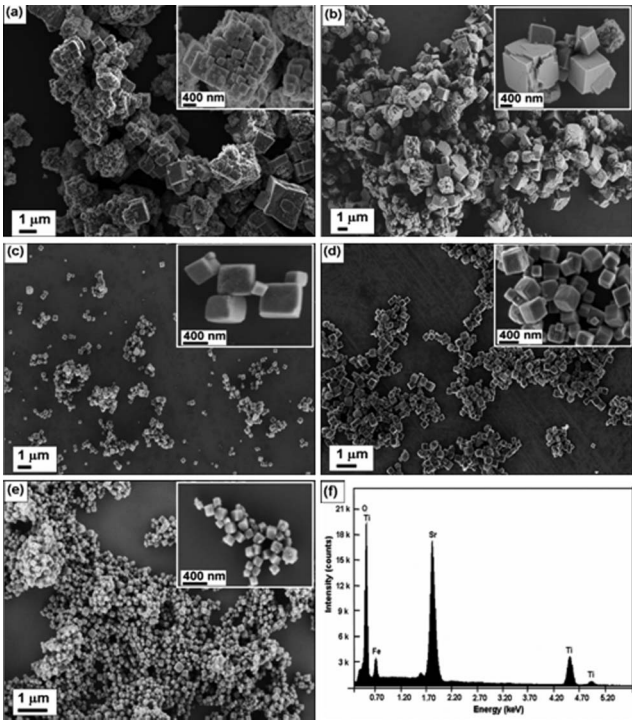

Fig. 5 SEM images of $SrTi_{1-x}Fe_xO_3$ samples: x = 0.0 (a), 0.05 (b), 0.1 (c), 0.25 (d), 0.4 (e); (f) EDX spectrum of the x = 0.25 sample.

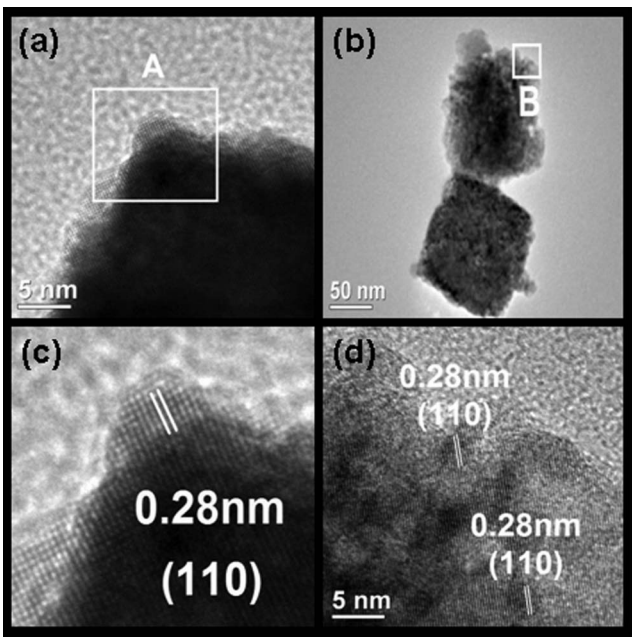

Fig. 6 (a) and (b) TEM images, (c) and (d) HRTEM images of the x = 0.4 sample.

contrast between the crystallites (see Fig. 6b and d) suggest the presence of nanopores which separate the primary particles. According to Calderone and co-workers,[14] aggregates formed by small nanocrystals with nanopores could be originated from an oriented attachment crystal growth mechanism initiated by a self-assembly process.[52]

According to the work of Alfredsson and co-workers,[39] the morphology of $CaTiO_3$ varied significantly in the presence of divalent dopant ions such as Fe^{2+}, Mg^{2+} and Ni^{2+}. Although in our samples the predominant oxidation state of iron was 2+, FE-SEM and TEM results showed that the morphology of the nanoparticles was not significantly affected by the substitution of titanium by iron atoms. We attribute this fact to the faster kinetics of crystal growth of the MAH method[27] compared to the flux grown single crystals method used by Alfredsson and co-workers to obtain $CaTiO_3$.

4. Conclusions

In summary, we have successfully synthesized STFO nanocubes using the MAH method at a relatively lower temperature and a shorter synthesis time. To the best of our knowledge, this is the first time that the STFO solid solution was obtained by using this methodology. XAS at the Fe K-edge measurements revealed that iron ions present a mixed Fe^{2+}/Fe^{3+} oxidation state and occupy Ti^{4+}-sites. XRD patterns and UV-visible spectra show that the addition of iron increases the lattice parameter, a, and reduces the optical gap of STFO samples. An analysis of FE-SEM and HRTEM images point out that, independently of iron content, the nanoparticles have a cube-like morphology and are formed by a self-assembly of small primary nanocrystals. These STFO nanocubes can be used to prepare thick films by tape casting or suspension methodology.

Acknowledgements

The authors are grateful to Mr Rorivaldo Camargo for operating the FE-SEM equipment and Dr Alexandre Mesquita for his help on the analysis of EXAFS data. We also acknowledge the financial support of the Brazilian agencies CNPq (project MCT/CNPq No. 70/2008) and FAPESP. The transmission electron microscopy work was performed on the JEM-2100 HT microscope at LME/LNNano/CNPEM. This research was partially developed at LNLS–National Laboratory of Synchrotron Light, Brazil. Juan Andrés acknowledges Generalitat Valenciana (Prometeo/2009/053 project), Ministerio de Ciencia e Innovación (CTQ2009-14541-Co2 project) Programa de Cooperación Científica con Iberoamerica (Brazil), and Ministerio de Educación (PHB2009-0065-PC project).

References

1 P. Meuffels, *J. Eur. Ceram. Soc.*, 2007, **27**, 285–290.
2 G. Neri, G. Micali, A. Bonavita, R. Licheri, R. Orru, G. Cao, D. Marzorati, E. M. Borla, E. Roncari and A. Sanson, *Sens. Actuators, B*, 2008, **134**, 647–653.
3 G. Jin, G. Choi, W. Lee and J. Park, *J. Nanosci. Nanotechnol.*, 2011, **11**, 1738–1741.
4 H.-S. Kim, L. Bi, H. Paik, D.-J. Yang, Y. C. Park, G. F. Dionne and C. A. Ross, *Nano Lett.*, 2010, **10**, 597–602.
5 O. K. Tan and Y. Hu, *US Pat.*, 2011/0104002A1, 1=6, 2011.
6 L. H. Brixner, *Mater. Res. Bull.*, 1968, **3**, 299.
7 A. Rothschild, W. Menesklou, H. L. Tuller and E. Ivers-Tiffee, *Chem. Mater.*, 2006, **18**, 3651–3659.
8 M. Vracar, A. Kuzmin, R. Merkle, J. Purans, E. A. Kotomin, J. Maier and O. Mathon, *Phys. Rev. B: Condens. Matter Mater. Phys.*, 2007, **76**, 12.
9 Y. Hu, O. K. Tan and W. G. Zhu, *IEEE Sens. J.*, 2006, **6**, 1389–1394.

10 Y. G. Sun and Y. N. Xia, *Science*, 2002, **298**, 2176–2179.
11 S. Deville, E. Maire, G. Bernard-Granger, A. Lasalle, A. Bogner, C. Gauthier, J. Leloup and C. Guizard, *Nat. Mater.*, 2009, **8**, 966–972.
12 S. M. Woodley and R. Catlow, *Nat. Mater.*, 2008, **7**, 937–946.
13 U. Banin, *Nat. Mater.*, 2007, **6**, 625–626.
14 J. Yang and J. Y. Ying, *Nat. Mater.*, 2009, **8**, 683–689.
15 A. Pyatenko, M. Yamaguchi and M. Suzuki, *J. Phys. Chem. C*, 2007, **111**, 7910–7917.
16 C. Burda, X. B. Chen, R. Narayanan and M. A. El-Sayed, *Chem. Rev.*, 2005, **105**, 1025–1102.
17 J. A. Dahl, B. L. S. Maddux and J. E. Hutchison, *Chem. Rev.*, 2007, **107**, 2228–2269.
18 A.-H. Lu, E. L. Salabas and F. Schueth, *Angew. Chem., Int. Ed.*, 2007, **46**, 1222–1244.
19 S. Berger and Y. Drezner, *Ferroelectrics*, 2005, **327**, 85–89.
20 X. G. Peng, L. Manna, W. D. Yang, J. Wickham, E. Scher, A. Kadavanich and A. P. Alivisatos, *Nature*, 2000, **404**, 59–61.
21 X. Zhang, P. Hu, Y. B. Cao, W. C. Xiang, M. S. Yao, H. B. Zhang, F. L. Yuan and R. F. Xu, *CrystEngComm*, 2011, **13**, 3057–3063.
22 D. Alloyeau, C. Ricolleau, C. Mottet, T. Oikawa, C. Langlois, Y. Le Bouar, N. Braidy and A. Loiseau, *Nat. Mater.*, 2009, **8**, 940–946.
23 L. F. da Silva, L. J. Q. Maia, M. I. B. Bernardi, J. A. Andres and V. R. Mastelaro, *Mater. Chem. Phys.*, 2011, **125**, 168–173.
24 L. F. da Silva, M. I. B. Bernardi, L. J. Q. Maia, G. J. M. Frigo and V. R. Mastelaro, *J. Therm. Anal. Calorim.*, 2009, **97**, 173–177.
25 L. J. Q. Maia, J. Fick, C. Bouchard, V. R. Mastelaro, A. C. Hernandes and A. Ibanez, *Opt. Mater.*, 2010, **32**, 484–490.
26 W. Avansi, Jr., C. Ribeiro, E. R. Leite and V. R. Mastelaro, *J. Cryst. Growth*, 2010, **312**, 3555–3559.
27 I. Bilecka and M. Niederberger, *Nanoscale*, 2010, **2**, 1358–1374.
28 S. Komarneni, R. Roy and Q. H. Li, *Mater. Res. Bull.*, 1992, **27**, 1393–1405.
29 M. L. Moreira, J. Andres, J. A. Varela and E. Longo, *Cryst. Growth Des.*, 2009, **9**, 833–839.
30 M. Godinho, C. Ribeiro, E. Longo and E. R. Leite, *Cryst. Growth Des.*, 2008, **8**, 384–386.
31 M. L. Moreira, E. C. Paris, G. S. do Nascimento, V. M. Longo, J. R. Sambrano, V. R. Mastelaro, M. I. B. Bernardi, J. Andres, J. A. Varela and E. Longo, *Acta Mater.*, 2009, **57**, 5174–5185.
32 D. P. Volanti, M. O. Orlandi, J. Andres and E. Longo, *CrystEngComm*, 2010, **12**, 1696–1699.
33 C. Yang, X. Su, F. Xiao, J. Jian and J. Wang, *Sens. Actuators, B*, 2011, **158**, 299–303.
34 I. Bilecka, I. Djerdj and M. Niederberger, *Chem. Commun.*, 2008, 886–888.
35 C. O. Kappe, *Chem. Soc. Rev.*, 2008, **37**, 1127–1139.
36 S. H. Jhung, T. Jin, Y. K. Hwang and J.-S. Chang, *Chem.–Eur. J.*, 2007, **13**, 4410–4417.
37 G. A. Tompsett, W. C. Conner and K. S. Yngvesson, *ChemPhysChem*, 2006, **7**, 296–319.
38 M. L. Moreira, J. Andres, V. R. Mastelaro, J. A. Varela and E. Longo, *CrystEngComm*, 2011, **13**, 5818–5824.
39 M. Alfredsson, F. Cora, D. P. Dobson, J. Davy, J. P. Brodholt, S. C. Parker and G. D. Price, *Surf. Sci.*, 2007, **601**, 4793–4800.
40 H. P. Klug and L. E. Alexander, *X-ray Diffraction Procedures: For Polycrystalline and Amorphous Materials*, Wiley–Interscience, New York, USA, 1974.
41 K. Olimov, M. Falk, K. Buse, T. Woike, J. Hormes and H. Modrow, *J. Phys.: Condens. Matter*, 2006, **18**, 5135–5146.
42 A. Michalowicz, J. Moscovici, D. Muller-Bouvet and K. Provost, in *14th International Conference on X-Ray Absorption Fine Structure*, ed. A. DiCicco and A. Filipponi, IOP Publishing Ltd, Bristol, 2009, **vol. 190**.
43 A. L. Ankudinov, B. Ravel, J. J. Rehr and S. D. Conradson, *Phys. Rev. B: Condens. Matter Mater. Phys.*, 1998, **58**, 7565–7576.
44 D. L. Wood and J. Tauc, *Phys. Rev. B: Solid State*, 1972, **5**, 3144.
45 R. D. Shannon, *Acta Crystallogr., Sect. A: Cryst. Phys., Diffr., Theor. Gen. Crystallogr.*, 1976, **32**, 751–767.
46 G. Neri, A. Bonavita, G. Micali, G. Rizzo, R. Licheri, R. Orru and G. Cao, *Sens. Actuators, B*, 2007, **126**, 258–265.
47 T. R. Clevenger, *J. Am. Ceram. Soc.*, 1963, **46**, 207–210.
48 T. Yamamoto, *X-Ray Spectrom.*, 2008, **37**, 572–584.
49 M. D. Drahus, P. Jakes, E. Erdem and R. A. Eichel, *Solid State Ionics*, 2011, **184**, 47–51.
50 E. Orhan, F. M. Pontes, C. D. Pinheiro, T. M. Boschi, E. R. Leite, P. S. Pizani, A. Beltran, J. Andres, J. A. Varela and E. Longo, *J. Solid State Chem.*, 2004, **177**, 3879–3885.
51 L. Zhou and P. O'Brien, *Small*, 2008, **4**, 1566–1574.
52 H. Colfen and M. Antonietti, *Angew. Chem., Int. Ed.*, 2005, **44**, 5576–5591.
53 R.-Q. Song and H. Coelfen, *Adv. Mater.*, 2010, **22**, 1301–1330.
54 Y. Liu, Y. Zhang, H. Tan and J. Wang, *Cryst. Growth Des.*, 2011, **11**, 2905–2912.